Lecture Notes

Compuational Physics

(part of **Mathematical Methods & Computational Physics: PH33008/PH43018**)

S. Murugesh

January 19, 2009

Contents

Chapter 1

Differential equations:

Note: Usual notations

$$y_x = \frac{dy}{dx}; \quad y_{xxxxxxxxxx} = \frac{d^{10}y}{dx^{10}} = y_{10x}$$

1.1 Euler method

First step in solving differential equations. Consider

$$y_t = F(y(t), t) \; ; \quad y(t_0) = y_0. \tag{1.1}$$

Recall

$$y_t(t) = \lim_{\Delta\tau \to 0} \frac{y(t+\Delta\tau) - y(t)}{\Delta\tau} \tag{1.2}$$

$$\simeq \quad \frac{y(t+\Delta\tau) - y(t)}{\Delta\tau} \tag{1.3}$$

for small values of $\Delta\tau$. So,

$$y(t+\Delta\tau) = y(t) + \Delta\tau y_t(t). \tag{1.4}$$

Or

$$y(t_0+\Delta\tau) = y(t_0) + \Delta\tau y_t(t)|_{t_0}. \tag{1.5}$$

$$= y(t_0) + \Delta\tau F(y(t_0), t_0) \tag{1.6}$$

for small values of $\Delta\tau$.

Alternatively, recall Taylor expansion for $y(t)$ around t (for small $\Delta\tau$):

$$y(t+\Delta\tau) = y(t) + y_t(t)\Delta\tau + \frac{1}{2}y_{tt}\Delta\tau^2 + \frac{1}{6}y_{3t}\Delta\tau^3 + ... \tag{1.7}$$

$\rightarrow$ agrees with Eq. (1.5) to first order in $\Delta\tau$. So error in Euler method is of order $\Delta\tau^2$.

Pictorially, Euler method is shown in Figure 1. Euler method uses slope at the point t_0 to extrapolate $y(t_0 + \Delta\tau)$.

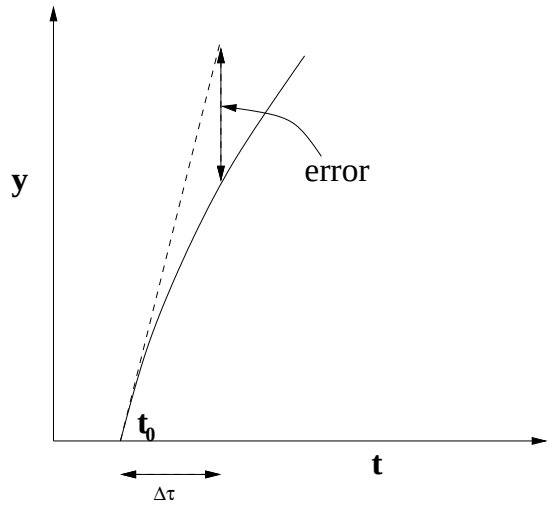

Figure 1.1: Euler method: Using $y(t_0)$ and the slope ($y_t(t_0)$), Euler method estimates $y(t_0+\Delta\tau)$ as $y(t_0)+y_t(t_0)\Delta\tau$. This agrees with Taylor series up to first order in $\Delta\tau$. Thus error is of order $\Delta\tau^2$.

1.2 Runge-Kutta method(s)

A more accurate method comes by choosing an intermediate point in the $'t'$ interval, say $\Delta\tau/2$, to calculate the slope, i.e., $F(y,t)$. The catch: to calculate $y(t_0+\frac{\Delta\tau}{2})$ use Euler method. So

Step 1:

$$y(t_0+\frac{\Delta\tau}{2}) = y(t_0) + F(y(t_0),t_0)\Delta\tau. \tag{1.8}$$

Step2:

$$\begin{aligned} y(t_0+\Delta\tau) &= y(t_0) + y_t(t_0+\frac{\Delta\tau}{2})\Delta\tau \\ &= y(t_0) + F(y(t_0+\frac{\Delta\tau}{2}), t_0+\frac{\Delta\tau}{2})\Delta\tau. \end{aligned} \tag{1.9}$$

Or, in conformity with texts,

Step 1:

$$K_1 = F(y(t_0),t_0)\Delta\tau \tag{1.10}$$

Step 2:

$$K_2 = F(y(t_0)+\frac{K_1}{2}, t_0+\frac{\Delta\tau}{2})\Delta\tau \tag{1.11}$$

$$y(t_0+\Delta\tau) = y(t_0) + K_2. \tag{1.12}$$

This is the Two-step(for obvious reasons) Runge-Kutta method.

Exercise 1.1 *Find out the order of error in this method, upon comparing with Taylor series.*

Higher order methods follow on similar lines using more intermediate points to calculate the slope, with the Four-step RK method (or Fourth order RK method) being the preferred choice:

$$K_1 = F(y(t_0), t_0)\Delta\tau \tag{1.13}$$

$$K_2 = F(y(t_0) + \frac{K_1}{2}, t_0 + \frac{\Delta\tau}{2})\Delta\tau \tag{1.14}$$

$$K_3 = F(y(t_0) + \frac{K_2}{2}, t_0 + \frac{\Delta\tau}{2})\Delta\tau \tag{1.15}$$

$$K_4 = F(y(0) + K_3, t_0 + \Delta\tau)\Delta\tau \tag{1.16}$$

$$y(t_0 + \Delta\tau) = y(t_0) + \frac{1}{6}(K_1 + 2K_2 + 2K_3 + K_4) \tag{1.17}$$

Exercise 2.2 *Radioactive decay is governed by the equation*

$$\frac{dN}{dt} = -\frac{N}{\tau}, \tag{1.18}$$

where $N(t)$ is the number of nuclei of the radioactive material at time $'t'$ and τ is the time constant for the decay. Choosing $N(0) = 100$ and $\tau = 1$, simulate Eq. (1.18) and compare with the analytical solution (How else can you verify?).

Exercnse 2.3 *Extend the scheme suggested by Euler's method to a) Coupled system of ODEs, b) Higher order ODEs and c) PDEs.*

Chapter 2

Projectiles

2.1 The cyclist: without resistance

Consider equation of motion

$$v_t = \frac{F}{m} \tag{2.1}$$

for a bicycle of velocity $v(t)$ and mass (including cyclist) m. F is the force acting on the bicycle, due to the cyclist's effort. Assume, horizontal road, and no resistance (anywhere). F is difficult to calculate. Let P be the power a cyclist can provide (can be roughly calculated experimentally). Then

$$P = E_t, \tag{2.2}$$

where E is the energy of the bicycle-cyclist combo. Road being horizontal, $E = mv^2/2$. Thus

$$P = mvv_t, \tag{2.3}$$

or

$$v_t = \frac{P}{mv}. \tag{2.4}$$

If P is constant then, if $v(0) = v_0$,

$$v = \sqrt{v_0^2 + 2Pt/m}. \tag{2.5}$$

Exercise 2.1: *Verify Eq. (2.5).*

Eq. (2.5) implies v increases indefinitely with time. Cannot be true.

Exercise 2.2: *Numerically simulate Eq. (2.4), assuming $P = 400W$ (constant!), and other values reasonably.*

2.2 The cyclist: with resistance

Assume air resistance of the form

$$F_{drag} = B_1 v + B_2 v^2 \tag{2.6}$$

$$v_t = \frac{P}{mv} - F_{drag} \tag{2.7}$$

It turns out this is more significant compared to other resistance, such as friction between moving parts of the bicycle. The first term in Eq. (2.6) is the familiar Stokes' law behavior. The second term is naturally the next possible significant term (recall Taylor expansion). For large velocities the second term dominates. Roughly

$$B_2 = \rho A/2, \tag{2.8}$$

where ρ is the density of air and A the frontal area of the cyclist-bicycle combo.

The mass of air displaced by the cyclist $\rho Avdt$, carrying a K.E $\rho Avdt \cdot v^2/2$. This equals the work done by $F_{drag}(= F_{drag} \cdot vdt)$.

$$F_{drag} \cdot vdt = \frac{m_{air}}{2} v^2 \tag{2.9}$$

$$= \rho Avdt \cdot \frac{v^2}{2}. \tag{2.10}$$

So Eq. (2.4) modifies to (omitting the Stokes' term)

$$v_t = \frac{P}{mv} - \frac{\rho A}{2m} v^2. \tag{2.11}$$

Exercise 2.3: *Numerically plot the velocity of the cyclist using Eq. (2.11) for the same values for the parameters, and compare with the results for Exercise 2.2.*

2.3 2-D projectile motion

Consider projectile motion in 2-D - tracing the horizontal(x) and vertical(y) coordinates. The equation of motion is the system of two differential equations

$$x_{tt} = 0 \; ; \quad y_{tt} = -g. \tag{2.12}$$

Or,

$$x_t = v_x \tag{2.13}$$

$$v_{xt} = 0, \tag{2.14}$$

$$y_t = v_y, \tag{2.15}$$

$$v_{yt} = -g. \tag{2.16}$$

Note: In v_x and v_y, the subscripts are not derivatives.

Exercise 2.4: *Trace the projective described by the Eqs. (2.13-2.16), using Euler/R-K4 methods, choosing suitable initial values.Check if max range happens at angle of inclination of* 45^o.

2.4 Projectile including air resistance

Recall air resistance given by

$$F_{drag} = B_2 v^2 \ ; \quad v^2 = v_x^2 + v_y^2. \tag{2.17}$$

Evidently,

$$F_{drag,x} = F_{drag} \frac{v_x}{v} \tag{2.18}$$

$$F_{drag,y} = F_{drag} \frac{v_y}{v}. \tag{2.19}$$

Here again, subscripts do not denote derivatives
So, the modified equations are

$$x_t = v_x \tag{2.20}$$

$$v_{xt} = -\frac{B_2}{m} v v_x, \tag{2.21}$$

$$y_t = v_y, \tag{2.22}$$

$$v_{yt} = -g - \frac{B_2}{m} v v_y. \tag{2.23}$$

Exercise 2.5: *Repeat Exercise 2.4 for Eqs. (2.20-2.23), choosing a reasonable value for* $B_2 (= \rho A/2)$.

2.5 Projectile with density correction at high altitudes

In Eq. (2.23) B_2 depends on ρ. At high altitudes, however, ρ is low. Infact

$$\rho = \rho_0 \exp(-y/y_0) \tag{2.24}$$

with $y_0 = 1.0 \times \ 10^4 \ m$.

Exercise 2.6: *Repeat Exercise 2.5 for the same values, but incorporating density correction. Study carefully how the results vary.*

2.6 Motion of a batted baseball: Effect of velocity dependent drag, and wind

Base ball motion is complicated by the behavior of the ball with the speed. The behavior of the drag coefficient $C (B_2 = C\rho A)$ is given in Figure 2.1 (a rough sketch). The drag when air flow is smooth is more, and less when the air around the ball is turbulent. For a rough ball, the turbulent phase sets in at much lower velocities, while for a smooth ball this happens at high velocities.

An exact analytical function for the above form is nontrivial. However, numerically, the behavior for a normal baseball is reasonably well described by

$$\frac{B_2}{m} = 0.0039 + \frac{0.0058}{1 + \exp[(v - v_d)/\Delta]}, \tag{2.25}$$

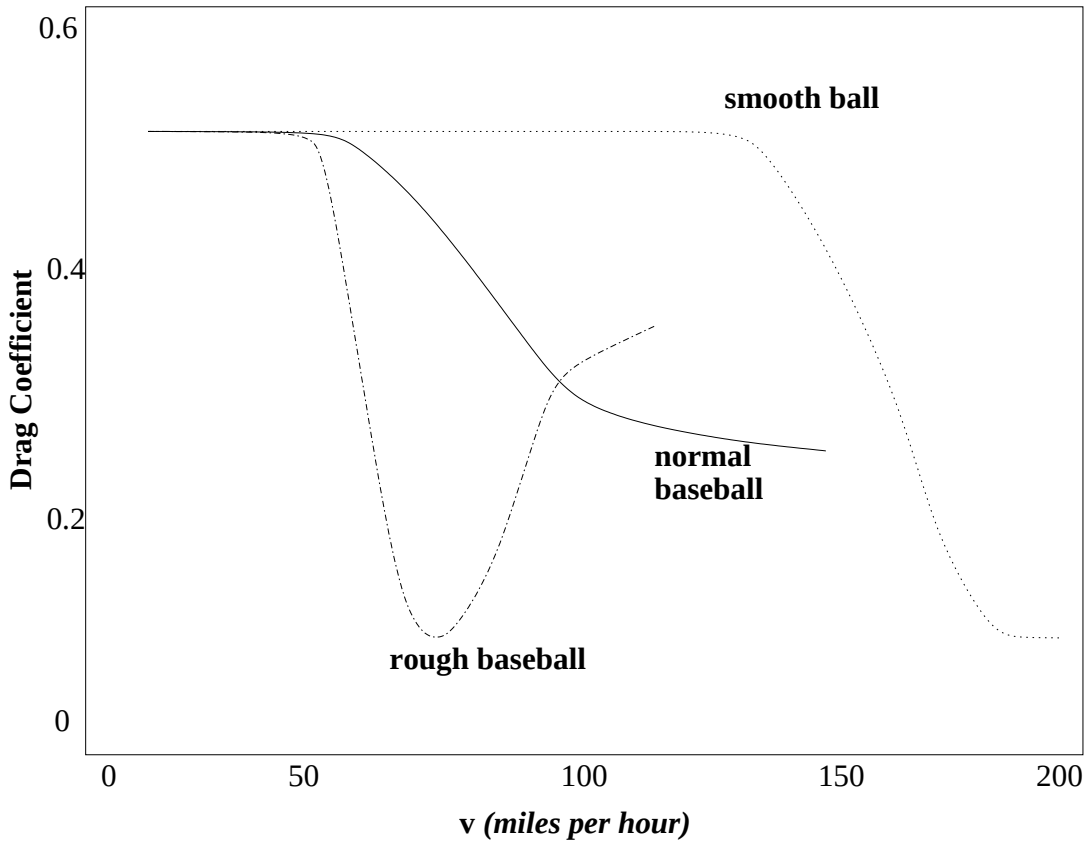

Figure 2.1: Behavior of the drag coefficient C is shown above for three different types of baseballs. A rough ball can cause the air around it to be turbulent at much lower velocities, compared to a smooth baseball. Note that for low velocities the coefficient is roughly 0.5, as was the case from our arguement for the cyclist.

where $v_d = 35\ m/s$ and $\Delta = 5\ m/s$.

Add to this the effect of wind, assuming the wind to be blowing horizontally, and having a constant magnitude and direction during the flight of the ball. Then (see Eq. (2.21) and Eq. (2.23)),

$$F_{drag,x} = -B_2|\vec{v} - \vec{v}_{wind}|(v_x - v_{wind}), \tag{2.26}$$

$$F_{drag,y} = -B_2|\vec{v} - \vec{v}_{wind}|v_y. \tag{2.27}$$

Exercise 2.7: *Trace the trajectories of a normal baseball, a) in vacuum, b) with a wind drag. Repeat the same assuming a wind speed of* $10mph$*. Of particular interest is the angle of maximum range, and the form of the trajectory.* $m = 149g$.

2.7 Motion of pitched baseball (knuckleball): Effect of spin

While all the features of the previous section follows for a pitched baseball, the primary difference is the effect of spin. It turns out that the force on the ball due to its spin is the most significant in changing its trajectory. The force can be understood from the drag force F_{drag} on the two sides of the ball. Let y axis, as earlier, be the direction of vertical. Consider the baseball moving along the x axis with velocity v, and spinning with the axis along y as shown in the Figure 2.2.

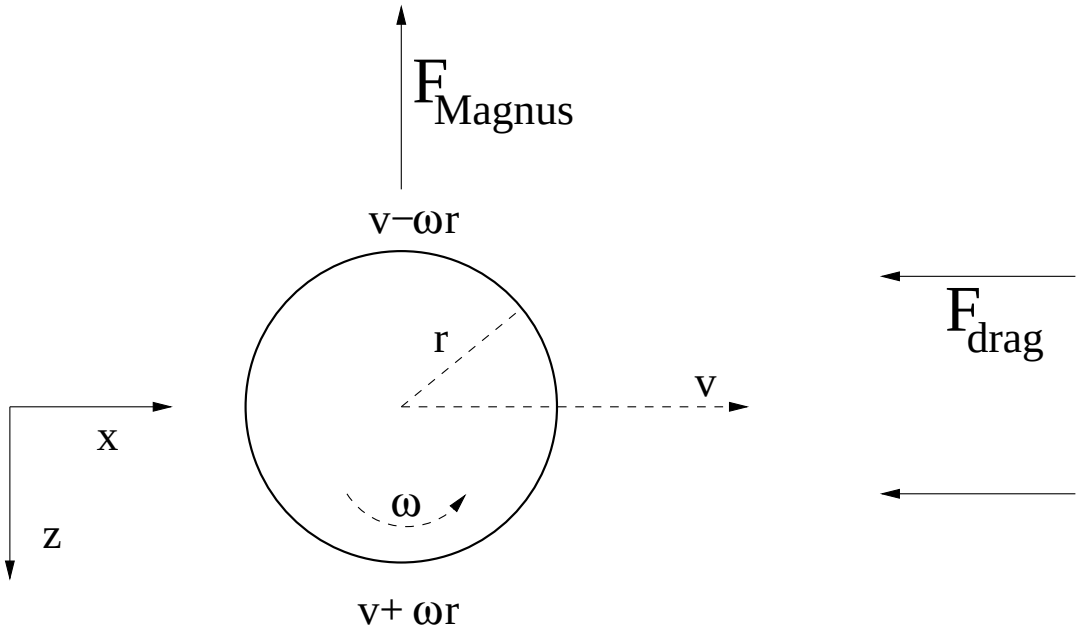

Figure 2.2: Schematic picture of the spinning ball, and the relative velocity on the two sides with respect to the wind. This leads to a difference in the drag force on the two sides, effectively leading to the Magnus force F_{Magnus} in the $-z$ direction. y axis is the vertical direction, which is also the direction of spin.

From the figure

$$F_{Magnus} = -S_0 \omega v_x \hat{\mathbf{z}} \; ; \quad (S_0 \vec{\omega} \times \vec{v} \;\; in \; general), \tag{2.28}$$

and the trajectory is 3-dimensional. So the equations become

$$x_t = v_x \tag{2.29}$$

$$v_{xt} = -\frac{B_2}{m} v v_x, \tag{2.30}$$

$$y_t = v_y, \tag{2.31}$$

$$v_{yt} = -g \tag{2.32}$$

$$z_t = v_z, \tag{2.33}$$

$$v_{zt} = -\frac{S_0 \omega v_x}{m}. \tag{2.34}$$

Experimentally, $S_0/m(\approx 4.1 \times 1)^{-4}$, where $m = 149g$.

2.8 Trajectory of a Golf ball:

Little change in detail, the spin is along the z axis. Thus the trajectory is 2-D with equations given by:

$$x_t = v_x \tag{2.35}$$

$$v_{xt} = -\frac{B_2}{m} v v_x - \frac{S_0 \omega v_y}{m}, \tag{2.36}$$

$$y_t = v_y, \tag{2.37}$$

$$v_{yt} = -\frac{B_2}{m} v v_y + \frac{S_0 \omega v_x}{m} - g. \tag{2.38}$$

Recall, $B_2 = C\rho A$. Experimentally,

$$\begin{aligned} C = 0.5 \ &: \ v < 14m/s \\ = 7/v \ &: \ v > 14m/s \end{aligned} \tag{2.39}$$

$$S_0 \omega / m = 0.25 s^{-1}. \tag{2.40}$$

Exercise 2.8: *Consider a cricket ball bowled along the x direction, with its seam in the $x - y$ plane, with y along the vertical. One side of the ball is assumed to be smooth compared to the other. If the ball is bowled with a backspin (angular velocity along z direction), sketch a rough force diagram, and write down the equations of motion for the ball. Which direction do you expect the swing to be?*

Suggested reading: See the short writeup on *The physics of football* in Physics World, June 1, 1998: http://physicsworld.com/cws/article/print/1533

Chapter 3

Oscillatory motion and Chaos

Notation:

$$\dot{y} = \frac{dy}{dt}; \quad \dddot{y} = \frac{d^3y}{dt^3} = y_{3t}$$

3.1 Simple harmonic motion:

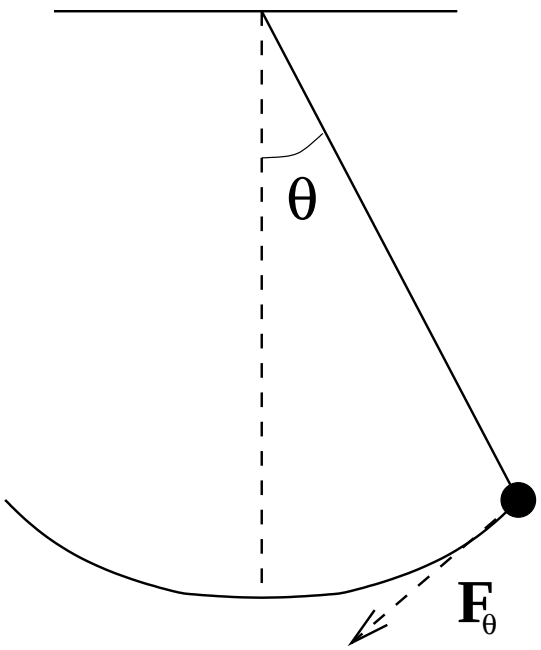

Figure 3.1: A simple pendulum. As long as oscillations remain small, the equation of motion is $F_\theta = -mg\theta$. Otherwise, $F_\theta = -mg\sin\theta$, a more complex nonlinear system. In particular, the period of the nonlinear pendulum is not $2\pi\sqrt{l/g}$.

From Newton:

$$\ddot{\theta} = -\frac{g}{l}\theta. \tag{3.1}$$

Solution

$$\theta = \theta_0 \sin(\Omega t + \phi) \tag{3.2}$$

Numerical implementation: Rewrite the II order ODE as two first order ODE

$$\dot{\theta} = \omega \tag{3.3}$$

$$\dot{\omega} = -\frac{g}{l}\theta \tag{3.4}$$

Exercise 3.1: *Use methods discussed in Section 1 to numerically study the dynamics of the simple pendulum Eq. (3.3) and Eq. (3.4). How does the results from the two - Runge-Kutta and Euler - methods compare? The system is conservative with energy being the conserved quantity. Use this to check your numerical results. Also, compare with the analytical solution.*

Exercise 3.2: *How does the behavior change when θ in Eq. (3.4) is changed to $\sin\theta$. Once again, use (the new expression for) energy, the conserved quantity, to check your results.*

3.2 Driven nonlinear pendulum: Chaos

Deterministic systems have a predictable future, i.e., given the initial condition and forces on the system, the future of the system is *determined*. However, the system may be sensitively dependent on the initial conditions that predictions over long time is practically impossible without "precise" knowledge of the initial conditions. Simple example: A tossed coin, or dice. Nevertheless, given the forces and initial condition "precisely", the future of the system is "precisely" and "uniquely" determined. Two trajectories, very close to start with, can deviate away from each other *exponentially in time*, that soon they lose any semblance, owing to their *sensitive dependence on initial condition*- a fundamental feature of *Chaos*. An example can be found in the *driven nonlinear damped* pendulum

$$\ddot{\theta} = -\frac{g}{l}\sin\theta - q\dot{\theta} + F_D \sin(\Omega_D t). \tag{3.5}$$

Exercise 3.3: *Taking $l = g = 9.8$, $q = 1/2$ and $\Omega_D = 2/3$, obtain the trajectories of $\theta(t), \omega(t)$ for $F_D = 0, F_D = 0.5$ and $F_D = 1.2$ (See Figure 3.2). Note: $-\pi \leq \theta < \pi$. Take 'modulus' every time θ goes above π.*

Notice that the system has two periods, the characteristic period $T = 2\pi\sqrt{l/g}$ for small oscillations, and frequency of the driving force Ω_D. In the absence of the driving force, the system relaxes to a stop, $\dot{\theta} = 0$, due to the dissipation term. As the driving force F_D is increased (0.5) the system shows periodic motion, with period Ω_D of the driving force. On further increasing $F_D(= 1.2)$, the system shows chaotic behavior.

Exercise 3.4: *Consider two driven nonlinear pendulum θ_1 and θ_2 obeying the same dynamical equation, Eq. (3.5), with all parameters same, but differing slightly in their initial conditions. Let $\Delta\theta = |\theta_1 - \theta_2|$. Plot $\Delta\theta$ vs t for the values $F_D = 0.5$ and $F_D = 1.2$.*

Exercise 3.5: *Notice that for $F_D = 1.2$ in Exercise 3.4 the trajectory θ vs t is chaotic. Repeat Exercise 3.4 for different choices of (θ_1, θ_2). Plot average $\Delta\theta$ vs t, and find the slope of the line joining the maxima. The slope is the* **Lyapunov** *exponent of the system. Notice that it is $+ve$ when $F_D = 1.2$ and $-ve$ when $F_D = 0.5$. A positive Lyapunov exponent signifies* **Chaos**.

Exercise 3.6: *Using results from Exercise 3.4, plot the phase-space trajectories, i.e., ω vs θ (See Figure 3.3).*

3.3 Poincaré section

For $F_D = 0.5$, the system shows periodic behavior, and for large values of F_D, it shows chaotic behavior. Given that the system has a characteristic time period due to Ω_D, we can look at snapshots of the system, a stroboscopic plot, taken at regular intervals of time $2\pi/\Omega_D$. This stroboscopic phase-space plot in the characteristic time period of the system is known as *Poincaré section* or a *Poincaré surface*. For a periodic system, such as Eq. (3.5) for $F_D = 0.5$, this is just a point in the $\omega - \theta$ plane. For a chaotic system, the Poincaré map shows more structure and, is the same for a wide range of initial conditions. The system starting in any initial condition will sooner or later reach one of these points, and thus have the same same Poincareé surface. Thus for a chaotic system, *the Poincaré section is an invariant for a system, irrespective of the initial condition.* I.e., no matter what the initial condition, after a transient phase, the system goes into a phase such that the Poincaré section is the same. For this reason we say the surface is an *attractor*. For the periodic case, the surface is just a point. For the chaotic regime, the structure is more complex, referred to as the *strange attractor*.

Exercise 3.7: *Plot the Poincaré surface for the forced pendulum in the chaotic regime (See Figure 3.4). Change initial condition to confirm if the surface remains invariant.*

3.4 Period doubling map: Route to chaos

As F_D is increased further, the system again shows periodic behavior of period $2\pi/\Omega_D$. In fact still further it shows double, quadruple, and generally 2^n period behavior. This demonstrates *one way* the system evolves to a completely chaotic state. A nice way of studying this period doubling behavior is through the *bifurcation diagram*. The bifurcation diagram is a period map of θ vs F_D at intervals of $2\pi/\Omega_D$, after a transient phase. For values of F_D (such as 0.5) where the motion is periodic the plot is just the same point. For 2^n period, one has 2^n points.

Exercise 3.8: *Plot the bifurcation diagram for the forced pendulum for a range of values of F_D (See Figure 3.5).*

Though there is nothing universal in the way a system can reach a chaotic state, one thing universal about the bifurcation diagram is that the period window, i.e., the spacing between period doubling transitions rapidly becomes smaller with the order of transitions. Indeed, if F_n is the value of F_D at which transition to 2^n period behavior takes place, then

$$\delta_n \equiv \frac{F_n - F_{n-1}}{F_{n+1} - F_n} \tag{3.6}$$

approaches the Feigenbaum number (= 4.669..) for large n.

Exercise 3.9: *Using the bifurcation diagram obtained in Exercise 3.8, verify that δ_n approaches the Feigenbaum number.*

3.5 The Lorenz model

The Lorenz model is an oversimplified version of the Navier-Stokes equation applied to the case of Reyleigh-Bénard convection. Consider a fluid in a container with top and bottom surfaces held at different temperatures. As the difference in temperatures is slowly increased, the fluid goes from a stationary state, to steady flow (nonzero velocity field, but constant in time), to chaotic flow. The equations around the steady state are reduced to

$$\dot{x} = \sigma(y - x), \tag{3.7}$$

$$\dot{y} = -xz + rx - y, \tag{3.8}$$

$$\dot{z} = xy - bz. \tag{3.9}$$

Due to comparisons with a simplified model of the atmosphere, the Lorenz model is also referred to as the weather problem.

Exercise 3.10: *Show that the projection of the phase space plot in the $x - z$ plane has the butterfly structure shown below. The parameter values are $\sigma = 10$, $b = 8/3$ and $r = 25$ (See Figure 3.6).*

Exercise 3.11: *Obtain the Poincaré surface for the Lorenz model. Note that the system does not have a characteristic time period. The surface in this case is just the set of points on a plane that intersects the three dimensional trajectory, say, parallel to the $x-z$ plane at $y = 0$ (See Figures 3.7 & 3.8).*

3.6 The Billiard problem

Consider the trajectory of a billiard ball in a perfectly reflecting table. The motion is assumed to be frictionless, and the reflections are elastic. The equations are

$$\dot{x} = v_x, \tag{3.10}$$

$$\dot{y} = v_y. \tag{3.11}$$

At the point of reflection the tangential component of velocity is preserved, while the normal component is reversed. A typical trajectory for a square table is shown in Figure 3.9. The character of motion is governed by the shape of the table. In the case of a square and circular table the motion is noted to be periodic. A stadium is described as two halfs of a circle of radius r separated by a distance $2\alpha r$. The stadium billiard is chaotic for any nonzero value of α.

Exercise 3.12: *Simulate the trajectories of the billiard in the case of square, circle and stadium tables, and obtain the Poincaré surfaces.*

3.7 Bouncing balls

An ideal head on collision of a ball on another along the vertical direction, as shown in Figure 3.10, provides a simple example for chaotic motion.

The equations of motion in this case are given by

$$\dot{x}_1 = v_1 \ ; \quad \dot{v}_1 = -g; \tag{3.12}$$

$$\dot{x}_2 = v_2 \ ; \quad \dot{v}_2 = -g; \tag{3.13}$$

between collisions. At the point of collision between the two balls, the new velocities are dictated by conservation of momentum and energy. It is easy to verify that

$$v_{1,f} = \frac{m_1 - m_2}{m_1 + m_2} v_{1,i} + \frac{2m_2}{m_1 + m_2} v_{2,i}; \tag{3.14}$$

$$v_{2,f} = \frac{m_1 - m_2}{m_1 + m_2} v_{2,i} + \frac{2m_1}{m_1 + m_2} v_{1,i}; \tag{3.15}$$

At the time of collision of the ball of mass m_1 with the floor, the velocity is just reversed.

Exercise 3.13: *Plot the trajectories of x_1 as a function of time for three different cases, a) $m_2 = m_1$, b) $m_2 = 2m_1$ and c) $m_2 = 9m_1$. Also obtain the Poincaré section for the ball 2, when the ball 1 hits the floor.*

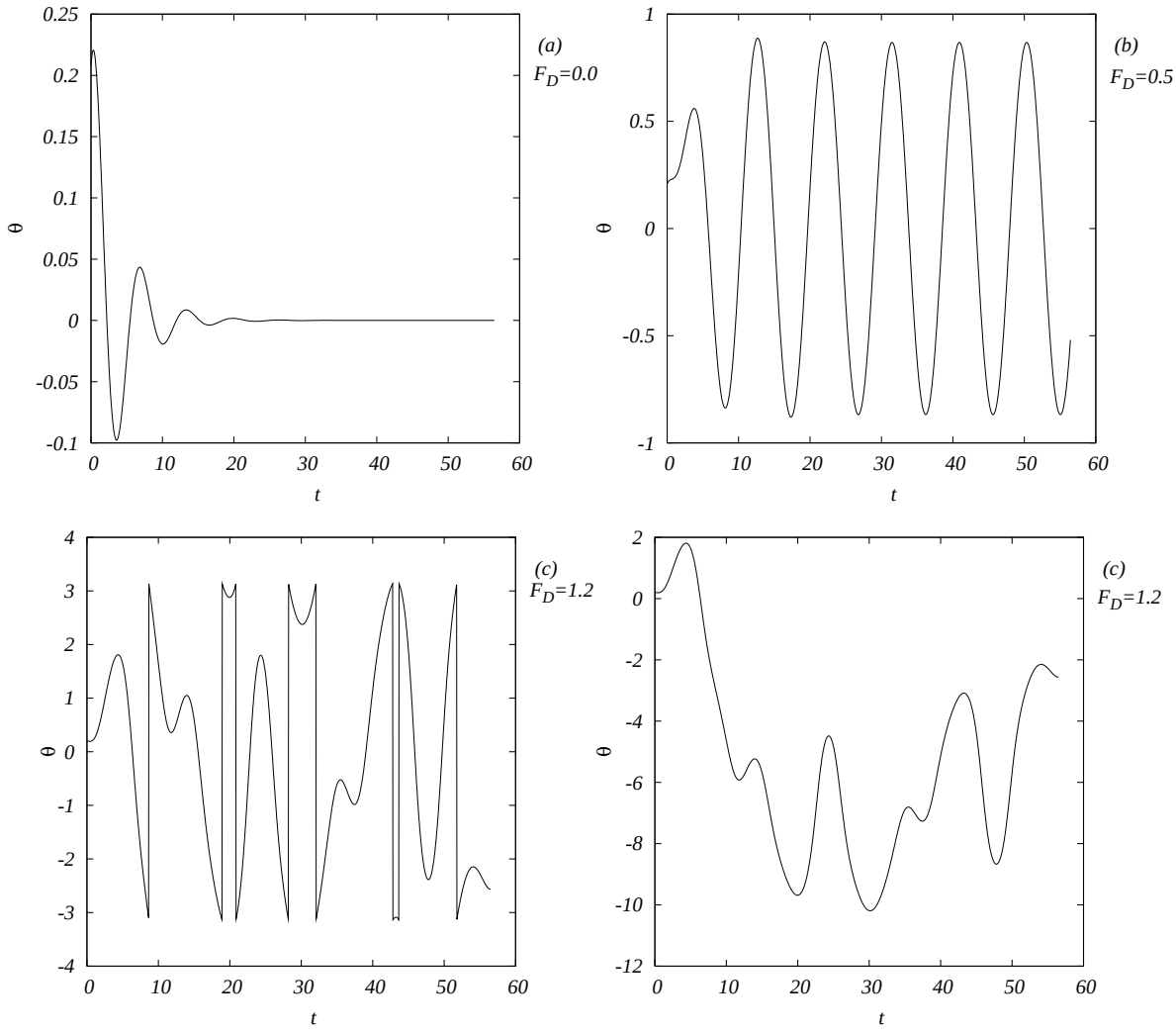

Figure 3.2: The trajectories of θ in time for three different values of the driving force. In (c), the abrupt jumps are due to the modulus on θ ($-\pi \leq \theta < \pi$). (d) is the same as (c), but without the modulus.

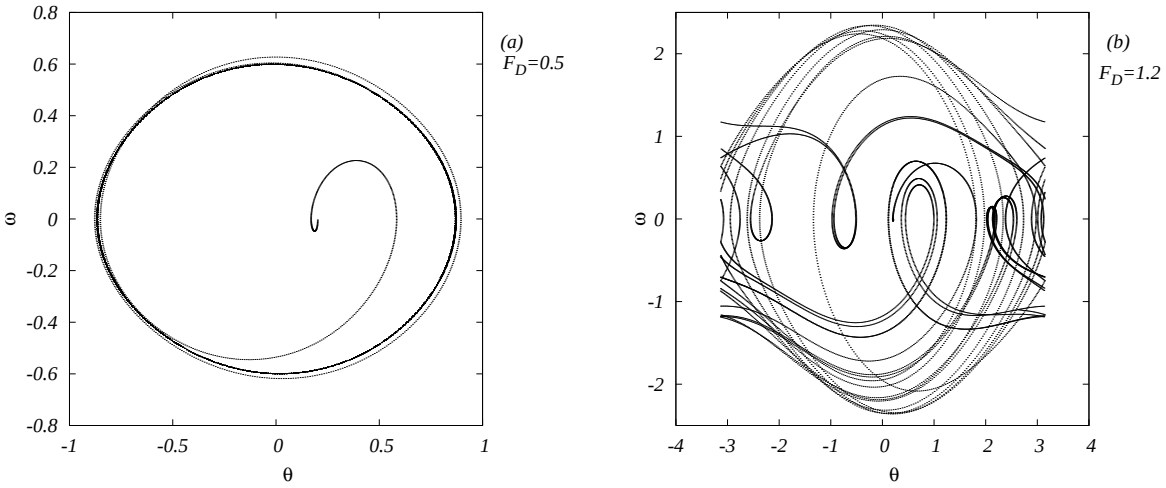

Figure 3.3: Poincaré surface for the driven pendulum at $F_D = 1.2$. (ω, θ) values at intervals of $2\pi/\Omega_D$, the period of the driving force. The plot is independent of the initial condition.

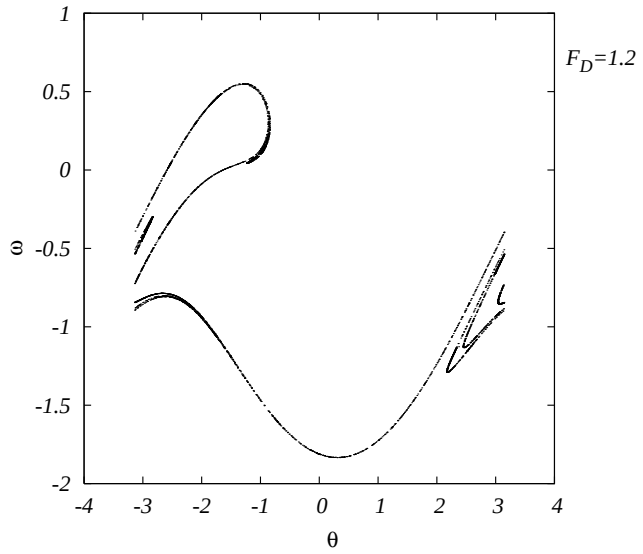

Figure 3.4: Poincaré surface for the driven pendulum at $F_D = 1.2$. (ω, θ) values at intervals of $2\pi/\Omega_D$, the period of the driving force. The plot is independent of the initial condition.

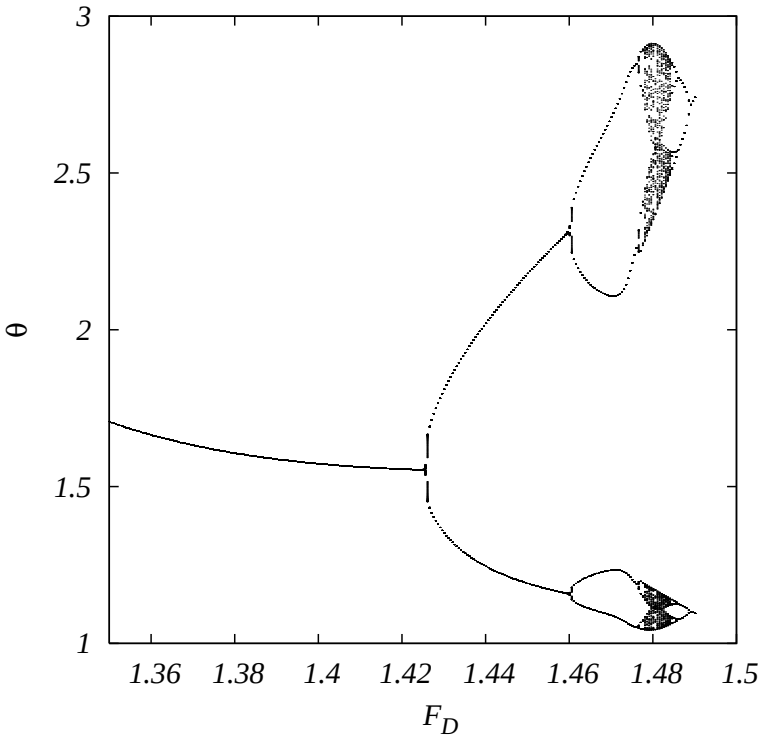

Figure 3.5: The bifurcation diagram for the period doubling as witnessed in the forced pendulum. The map is obtained by plotting values of θ at regular intervals of $2\pi/\Omega_D$ for over 500 periods, for each value of F_D.

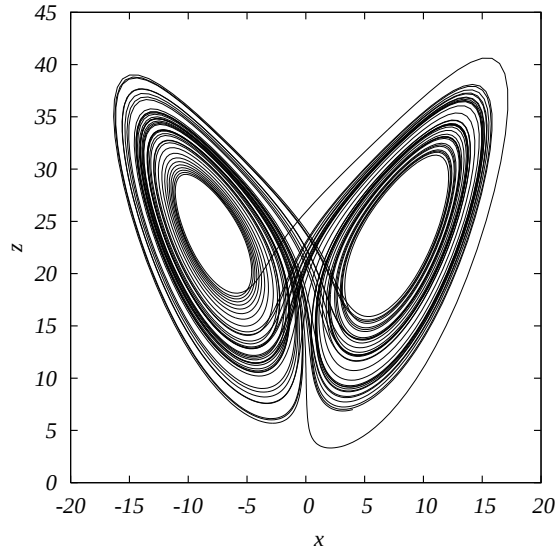

Figure 3.6: The *Butterfly* obtained as a phase portrait for the Lorenz model. The portrait is a projection in the $x - z$ plane of the three dimensional trajectory in the $x - y - z$ phase space. The parameter values are $\sigma = 10$, $b = 8/3$ and $r = 25$. The initial conditions chosen were $x = 1, y = 0 = z$.

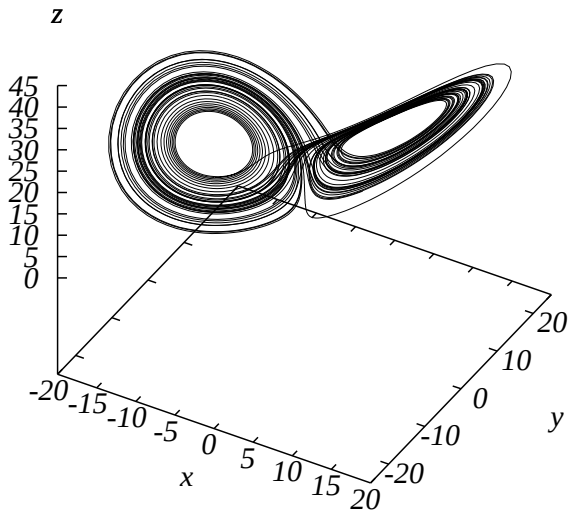

Figure 3.7: The trajectory in phase space for the Lorenz model for the same parametric values and initial conditions as in Figure 3.6. The Poincaré surface is the collection of points on the plane parallel to $x - z$ plane, that intersects the trajectory at $y = 0$ (See Figure 3.8).

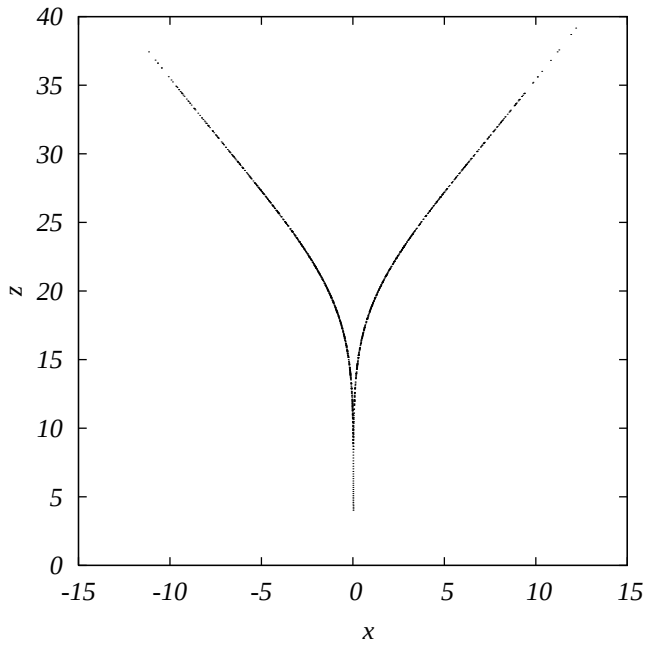

Figure 3.8: The trajectory in phase space for the Lorenz model for the same parametric values and initial conditions as in Figure 3.6. The Poincaré surface is the collection of points on the plane parallel to $x - z$ plane, that intersects the trajectory at $y = 0$ (See Figure 3.8).

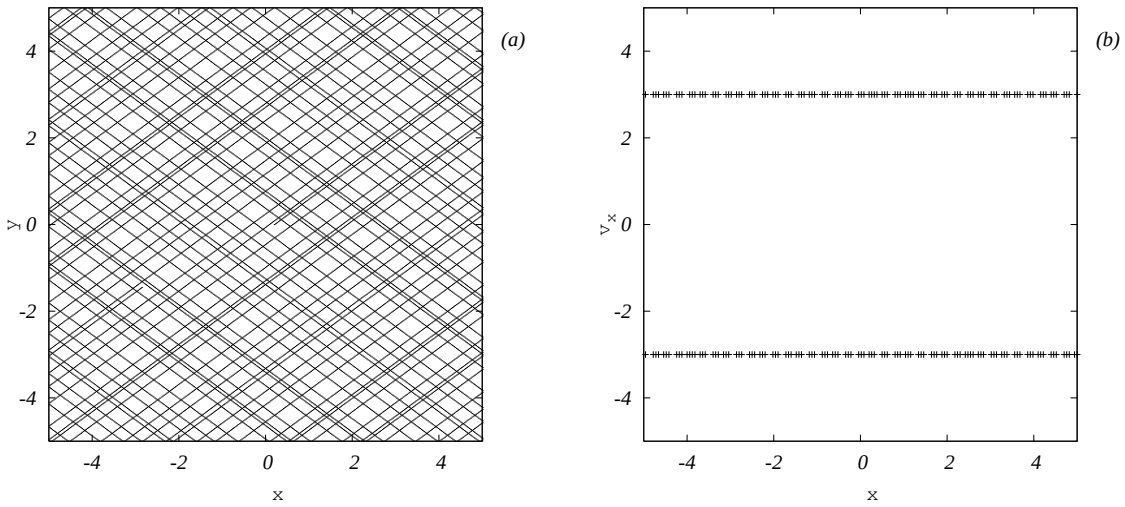

Figure 3.9: The trajectory of a billiard ball in a square billiard (a), with initial values $x = 0.2, y = 0, v_x = 3$ and $v_y = 2.2$, and the Poincaré surface. The Poincaré section is a plot in the $v_x - x$ space, when $y = 0$.

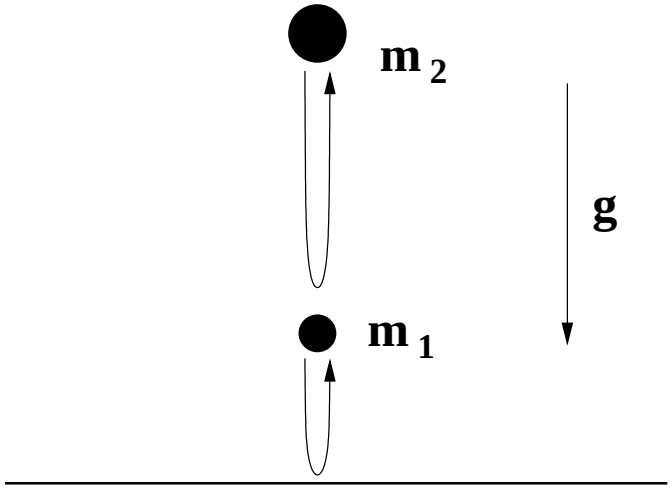

Figure 3.10: A ball of mass m_2 bounces *head on* from another ball of mass m_1, which in turn bounces of the floor. The collisions are assumed to be elastic, and ideally along the vertical. The system exhibits chaos depending on the ratio of the two masses.

Chapter 4

The solar system

In this chapter we look at tracking orbits of celestial bodies, and some related issues, numerically.

4.1 Kepler's laws

First off, motion of a planet around the Sun. The Sun is assumed to be massive enough compared to the planet (so it is!!), that we consider it to be fixed at the origin. The equations of motion for the planet are

$$\dot{x} = v_x \ ; \quad \dot{v}_x = -\frac{GM_S}{r^2} \cdot \frac{x}{r} \tag{4.1}$$

$$\dot{y} = v_y \ ; \quad \dot{v}_y = -\frac{GM_S}{r^2} \cdot \frac{y}{r} \tag{4.2}$$

Its worthwhile going to astronomical units, length in AU ($1AU = 1 \times 10^1 1\ m$, roughly the distance between Earth and Sun), and time in years. We know, for Earth, assuming circular orbit,

$$\frac{GM_S M_E}{r^2} = \frac{M_E v^2}{r} \tag{4.3}$$

$$\Rightarrow GM_S = 4\pi^2, \tag{4.4}$$

in astronomical units ($M_S = 2 \times 10^{30} Kg, M_E = 6 \times 10^{24} Kg$).

Exercise 4.1: *Obtain the orbits of Earth around the Sun, by appropriately choosing initial conditions for circular and elliptic orbits.*

Exercise 4.2: *Using the results obtained in Exercise 4.1 verify Kepler's laws of planetary motion.*

Exercise 4.3: *Without asking too many questions repeat exercises 4.1 and 4.2, assuming Newton's law were* $1/r^{2+\beta}$*, for* $\beta = .001, .01,$ *and* $.1$*, rest all remaining same.*

4.2 Precession of the perihelion of Mercury

Exercise 4.3, would've illustrated an unstable behavior of the orbit, wherein the orbit is seen to precess. A precession in the orbit of Mercury was a long standing fixation in celestial mechanics.

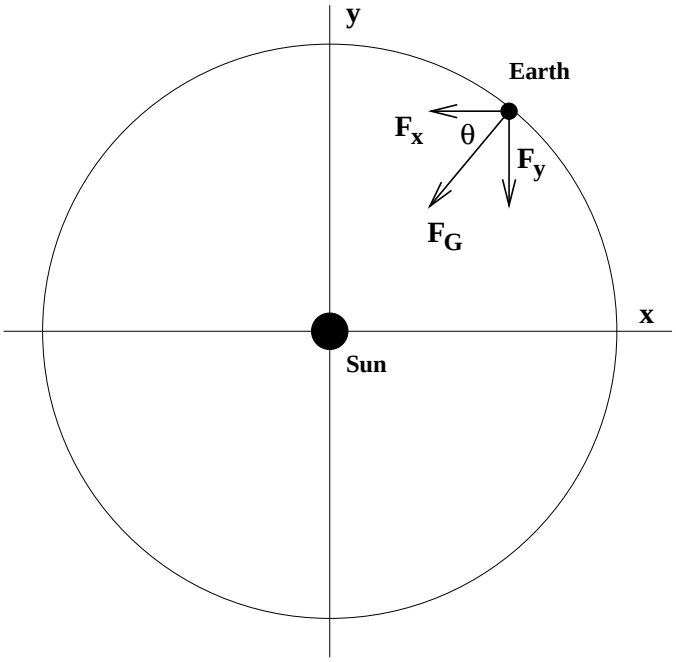

Figure 4.1: A schematic diagram showing the orbit of Earth around the Sun.

It was noticed that the orbit of Mercury precesses 566 *arcsecs* per century (1 $arcsec = 1/3600$ degrees). The Newton's law cannot be of the form $1/r^{2+\beta}$, $(\beta \neq 0)$, for various reasons. An alternate explanation was the effect of gravitational field of other planets on Mercury. This accounted for 523 *arcsecs/century* (This calculation was done *by hand* in the middle of 19^{th} century). The remaining 43 *arcsecs* were explained by the *general theory of relativity*, and was one more confirmation of the general theory itself. The force law according to general theory is

$$F_G \approx \frac{GM_S M_M}{r^2}(1 + \frac{\alpha}{r^2}) \tag{4.5}$$

where $\alpha \approx 1.1 \times 10^{-8} AU^2$. To study the behavior numerically for such a small value of α is not viable. The precession of the perihelion of Mercury due to the modified force law is calculated as follows:

1. Consider an elliptic orbit with semimajor axis $a = 0.39\ AU$ and eccentricity $e = 0.206$. Using conservation of energy and angular momentum, the velocity at aphelion can be obtained as

$$v = \sqrt{\frac{GM_S(1-e)}{a(1+e)}}. \tag{4.6}$$

2. Obtain the orbital trajectory for a fictional value of α, say 0.1.

3. A precessing orbit implies an aphelion (or perihelion) whose coordinate is changing with every revolution. Note down these coordinates (or angle), where the radial distance of Mercury from

the Sun is maximum (or minimum). Plot these extremal angle vs time. This is a straight line. The slope of this line gives the angular velocity, say ω_α, with which the orbit precesses, for the chosen value of α.

4. Repeat step 3 for different values of α, to obtain a set of values of ω_α for the corresponding values of α.

5. Plot ω_α vs α. This, again, is a straight line (why?). Find its slope $d\omega_\alpha/d\alpha$.

6. Using the slope obtained in the previous step, the precession for the real value of α is just $\alpha \times d\omega_\alpha/d\alpha$.

   Exercise 4.4: *Obtain the expression for velocity v, shown in step 1 above, at the aphelion.*

   Exercise 4.5: *Do steps 1 through 6 numerically, and show that the precession is indeed the missing 43 arcsecs/century (and thus provide the third supporting evidence for the general theory of relativity).*

   Exercise 4.6: *You could not have demonstrated this crucial confirmation of general theory so easily (as a text book exercise) had it not been for the straight line ω_α vs α. Why is it a straight line?*

4.3 The three-body problem: Effect of Jupiter on the orbit of Earth

So far we have looked at problems of the two-body central force kind. Here we look at the effect of the presence of an additional planet in the system, on the orbits of the first planet. We consider the Sun, Earth and Jupiter. The additional term in the scene is the force between Jupiter and Earth.

$$F_{EJ} = \frac{GM_J M_E}{r_{EJ}^2} \tag{4.7}$$

In component form (See Figure)

$$F_{EJ}, x = -\frac{GM_J M_E}{r_{EJ}^2}\cos\theta_{EJ} - \frac{GM_J M_E}{r_{EJ}^2}\frac{(x_E - x_J)}{r_{EJ}}. \tag{4.8}$$

$$F_{EJ}, y = -\frac{GM_J M_E}{r_{EJ}^2}\cos\theta_{EJ} - \frac{GM_J M_E}{r_{EJ}^2}\frac{(y_E - y_J)}{r_{EJ}}. \tag{4.9}$$

Use $GM_J = GM_S(M_J/M_S) = 4\pi^2 M_J/M_S, (M_J = 1.9 \times 10^{27} Kg)$ and radius 5.20 AU.

Exercise 4.7: *Making these modifications in the force equation for the two planets, study the trajectories of Earth and Jupiter around the Sun. Letting the mass of Jupiter to vary, at what ratio of M_J/M_E is there any perceivable difference in the orbit of the Earth? Try $M_J \rightarrow 1000\ M_J$.*

4.4 Resonances in the Solar system: Kirkwood Gaps and Planetary Rings

A curios hypothesis (a reminder of the way they did science those days) was the Titus-Bode formula (some time in the 18th century) for the radius of each planet, proposed without any scientific basis whatsoever. Hypothesis: The radius of planets around the Sun (in AU) were the related to the terms in the series $S_n = 0, 3, 6, 12, 24, ...$ as $r_n = (S_n + 4)/10$. This prediction agrees well for the first four planets. After a gap at $n = 5$ it agreed for Jupiter ($n = 6$) and Saturn. Uranus was discovered later (a search partially motivated by the Titus-Bode hypothesis). It does not agree so well for Neptune and Pluto however. The absence of any planet at $n = 5$ was a botheration. After several persistent searches for a missing planet, something was indeed observed at around 1800. But soon observations of several similar objects followed. These were realized as not planets really, and were named asteroids.

The explanation for the absence is the following. The radius of the orbit around the sun is also related to the period of the planet. The gap occurs at a radial distance such that the orbital period is half that of Jupiter. Implying that Jupiter's closest approach (and hence it significant gravitational pull) on such a planet will be at the same point on the planets orbit. Over several orbits, this distorts its orbit severely that eventually the planet's orbit is unstable. A smaller or larger orbit will not however face this problem, since the periods may not have such a simple ratio.

A correspondence of such gaps in the solar system can be seen with the sub system of Saturn and its moons. Due to Saturn's several moons, some orbits (or orbital radii) are not allowed. Objects in such an orbit will be pushed to take either a smaller or a larger orbit. This explains the phenomenon of several rings around Saturn, which are just a collection of celestial dust bodies in orbital motion around the planet. A detailed histogram of asteroids around Saturn shows gaps at certain radial distances, referred to as Kirkwood gaps. The gaps are referred to as 3/1, 5/2, 7/3, etc., based on the ratio of the orbital periods.

Exercise 4.7: The initial velocities of three asteroids, and Jupiter are $3.628 AU/yr, 3.471 AU/yr$, $3.267 AU/yr$ and $2.755 AU/yr$, and their radial distances 3 AU, 3.276 AU, 3.7 AU and 5.2 AU. Write the equations for orbital motion of the asteroids and Jupiter. The inter-asteroid gravitational force may be ignored in comparison with the force due to Jupiter and Sun.

4.5 Chaotic tumbling of Hyperion

Planetary motion also displays examples of synchronization and chaos. The planet is a more complex system than a point mass. An asymmetric mass distribution implies that two extreme ends of the planet are subjected to substantially different forces. If the outer end is sufficiently massive, this can lead to a compression of the planet, and *vice-versa*. As the planet rotates about its axis there is a constant churning of the planet leading to a mass redistribution. This changes the moment of inertia of the planet. Keeping the angular momentum constant thus implies a changing angular velocity. The effect of this change is so as to minimize the force gradient across the planet. This happens with the eventual synchronization of the period of rotation with the period of revolution. A well known example is the Moon with its same face looking down the Earth. Until this synchronization

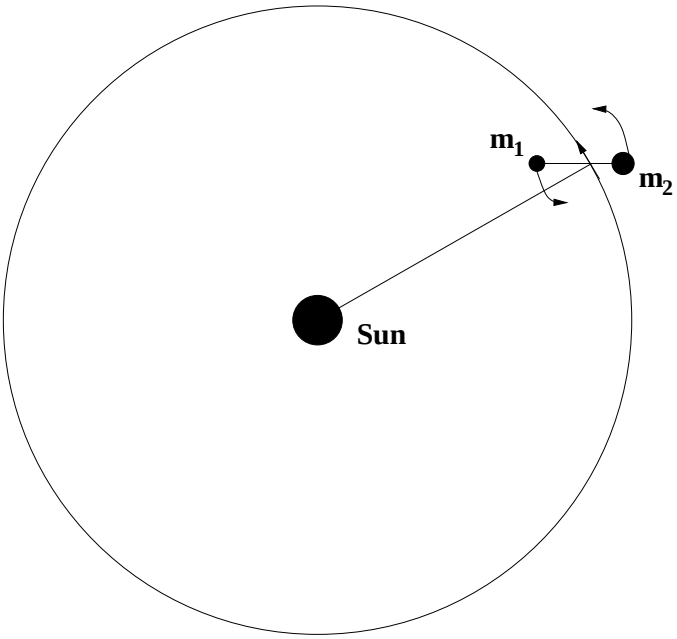

Figure 4.2: A simple model of a spatially extended planet. The planet is assumed to be a dumbbell made of two masses m_1 and m_2.

happens, or if the redistribution were not allowed, the motion of the celestial body is generally chaotic. Indeed, one of Saturn's moons is an example of such a body yet to synchronize, and hence showing chaotic motion.

A simpler model to demonstrate this is to consider a asymmetric dumbbell mass distribution of two point objects of mass m_1 and m_2, held at a constant distance apart, and orbiting a heavier body, as shown in Figure 4.2. The center of mass is governed by the same equations as in Eq. (4.1) and Eq. (4.2). Additionally, rotational angle θ of the dumbbell, is governed by the equations

$$\dot{\theta} = \omega, \tag{4.10}$$

$$\dot{\vec{\omega}} = \frac{\vec{\tau_1} + \vec{\tau_2}}{I}, \tag{4.11}$$

where

$$I = m_1((x_1 - x)^2 + (y_1 - y)^2) + m_2((x_2 - x)^2 + (y_2 - y)^2), \tag{4.12}$$

$$\vec{\tau_i} = [(x_i - x)\hat{\mathbf{i}} + (y_i - y)\hat{\mathbf{j}}] \times \vec{F_i}, \tag{4.13}$$

$$\vec{F_i} = -\frac{GM_S m_i}{r_i^3}(x_i\hat{\mathbf{i}} + y_i\hat{\mathbf{j}}), \tag{4.14}$$

and $i = 1, 2$.

Chapter 5

Potentials and Fields

Some problems in Electrostatics and Magnetostatics now. We start with

5.1 Laplace's equation (Relaxation methods)

$$V_{xx} + V_{yy} + V_{zz} = 0, \tag{5.1}$$

with some boundary conditions on a closed boundary region S, such as $V(S) = F(x, y, z)$. For practice lets consider 2-D. The method is same in 3 or more D. Firstly appreciate the difference between this problem, and the other ones implementable by the Euler's method: V is given on the boundary of a closed region, say on a circle or a square, and the problem is to find V in the region inside. This cannot be done by (at least a straight forward implementation of) the Euler method. The catch is to recall that the Laplacian is an averaging machine. If you consider a differential area (or volume), the value of V at the middle is just the average of V at points around it.

Let the problem be to solve the Laplace eqn., on a square($L \times L$), with boundary conditions

$$V(0, y) = 0 = V(x, 0), V(L, y) = V_0 = V(x, L). \tag{5.2}$$

The procedure will be to start with a grid

$$V(x, y) \rightarrow V[i, j] \; ; \quad i, j = 0.....N. \tag{5.3}$$

The initial conditions being

$$\begin{aligned} for \;\; i, j &= 0..N \\ if \;\; i * j &= 0 \\ V[i, j] &= 0 \\ if \;\; i = N \;\; or \;\; j &= N \\ V[i, j] &= V_0 \end{aligned}$$

The averaging is done in each element in the grid, except for the ones in the boundary.

Jordans method:

$$for \;\; i,j = 1...N-1$$
$$V_1[i,j] = \frac{V[i-1,j]+V[i+1,j]+V[i,j-1]+V[i,J+1])}{4}$$
$$V[\;\;] \leftarrow V_1[\;\;]$$

A better method (Gauss-Siedel):

$$for \;\; i,j = 1...N-1$$
$$V[i,j] = \frac{V[i-1,j]+V[i+1,j]+V[i,j-1]+V[i,J+1])}{4}$$

Still better:

$$V_{New}[i,j] = \alpha \Delta V[i,j] + V_{Old}[i,j]$$

$\alpha = 1$ is Gauss-Siedel method. $\alpha < 1$ is under relaxation, and $\alpha \geq 2$ is over relaxation: does not converge. Optimal $\rightarrow$ $1 \leq \alpha < 2$. For 2-D

$$\alpha \simeq \frac{2}{1+\pi/L}. \tag{5.4}$$

Exercise 5.1: *Find the potential in a square region of side* 1 *m, with the boundary condition* $V = -1$ *at* $(0,y)$ *and* $(y,0)$ *and* $V = 1$ *at* $(1,y)$ *and* $(x,1)$.

Exercise 5.2: *Find the potential in a square region of unit sides such that* $V = 0$ *on the boundary, and* $V = 1$, *for* $x = -1/4,\;\; -1/4 \leq y \leq 1/4$ *and* $V = -1$, *for* $x = 1/4,\;\; -1/4 \leq y \leq 1/4$ *(two thin plates of width* $1/2$ *held at potentials* $V = 1$ *and* $V = -1$, *respectively).*

Exercise 5.3: *Find the electric field in the square region for the problem in Exercise 5.2.*

5.2 Poisson's equation

$$V_{xx} + V_{yy} + V_{zz} = -\frac{\rho}{\epsilon_0}, \tag{5.5}$$

with suitable boundary conditions. The procedure is same as earlier, but for the additional term:

$$for \;\; i,j = 1...N-1$$
$$V[i,j] = \frac{V[i-1,j]+V[i+1,j]+V[i,j-1]+V[i,J+1])}{4} + \frac{\rho \Delta x^2}{4\epsilon_0}$$

5.3 Magnetic field due to a current

Take the simplest problem: the magnetic field at a point $(x,0)$ due to a long straight wire carrying current (along the $\hat{\mathbf{z}}$ direction). We know

$$d\vec{B} = \frac{\mu_0 I}{4\pi} \frac{\vec{dz} \times \vec{r}}{r^3}, \tag{5.6}$$

where all notations are clearly understandable. Only one component matters. The resultant field is given by

$$\vec{B} = \int_{-\infty}^{\infty} \frac{\mu_0 I}{4\pi} \frac{dz \sin\theta}{x^2 + z^2} \hat{\mathbf{y}}, \tag{5.7}$$

$$= \int_{-\infty}^{\infty} \frac{\mu_0 I}{4\pi} \frac{dzx}{(x^2 + r^2)^{3/2}} \hat{\mathbf{y}}, \tag{5.8}$$

Integration goes to summation:

$$\simeq \sum \frac{\mu_0 I}{4\pi} \frac{x\Delta z}{(x^2 + r^2)^{3/2}} \hat{\mathbf{y}}, \tag{5.9}$$

Exercise 5.4 *Find the potential and electric field everywhere inside cube of unit sides, with charge $q = 1$ at the center, for the boundary condition $V = 0$ on the six faces.*

5.4 Simpsons' rule

A more accurate way of performing are the Midpoint rule, Trapezium rule and Simpson's rule, in the increasing order of accuracy.

Midpoint rule:

$$\int_a^b f(x)dx = (b-a) f(\frac{a+b}{2}) \tag{5.10}$$

Trapezium rule:

$$\int_a^b f(x)dx = \frac{1}{2}(b-a)(f(a) + f(b)) \tag{5.11}$$

Simpson's rule:
Geometrically, we construct a quadratic function $Q(x)$ such that $Q(x) = f(x)$ at $x = a, x = b$ and $x = (a+b)/2$.

$$Q(x) = f(a)\frac{(x-m)(x-b)}{(a-m)(a-b)} + f(m)\frac{(x-a)(x-b)}{(m-a)(m-b)} + f(b)\frac{(x-a)(x-m)}{(b-a)(b-m)} \tag{5.12}$$

where $m = (a+b)/2$. Then

$$\int_a^b f(x)dx \simeq \int_a^b Q(x)\ dx \tag{5.13}$$

$$= \frac{b-a}{6}\big[f(a) + 4f(\frac{a+b}{2}) + f(b)\big]. \tag{5.14}$$

Exercise 5.5: *Obtain the expression in Eq. (5.12) for $Q(x)$ and verify the Simpson's integration formula Eq. (5.14).*

Exercise 5.6: *Use Simpson's rule to find the magnetic field at a point due a loop of current i.*

Chapter 6

Wave motion

In the previous chapter we saw some examples for static fields. Here we consider a wave equation to see how a dynamic field may be dealt with.

6.1 Simple wave equation

The first equation of wave motion is

$$\frac{\partial^2 y}{\partial t^2} = c^2 \frac{\partial^2 y}{\partial x^2}. \tag{6.1}$$

As a *linear* equation in 1-D this can be directly solved using Fourier transforms in principle, and in practice for many initial conditions. The usual complication arises when we deal with complicated initial/boundary conditions, or additional terms in the equation to represent more complex interactions. As a demo, we discretize the wave equation Eq. (6.1) to get

$$\frac{y(i,n+1) - 2y(i,n) + y(i,n-1)}{\Delta t^2} = c^2 \frac{y(i+1,n) - 2y(i,n) + y(i-1,n)}{\Delta x^2}, \tag{6.2}$$

or

$$y(i,n+1) = 2y(i,n) - y(i,n-1) + c^2 \frac{\Delta t^2}{\Delta x^2}[y(i+1,n) - 2y(i,n) + y(i-1,n)]. \tag{6.3}$$

So, to determine $\{y(i,n+1)\}$ one needs, $\{y(i,n)\}$ and $\{y(i,n-1)\}$. The initial profile of the wave gives $\{y(i,n)\}$ while, the initial velocity gives $\{y(i,n-1)\}$. Three different boundary conditions are usually employed: a) *Fixed boundary*: the points on the two ends of the string are fixed for all times, b) *Periodic boundary*: the points on the two ends of the string are equal (identified) for all times and c) *Free boundary*: the two end points are, well, *free* to vibrate as the dynamics dictates. The method works when $c^2\Delta t^2/\Delta x^2 = 1$. A better method will be to write the equation as

$$\frac{\partial^2 y}{\partial t^2} = c^2 \frac{y(i+1,n) - 2y(i,n) + y(i-1,n)}{\Delta x^2}, \tag{6.4}$$

and solve using Runge-Kutta method for second order partial differential equations.

6.2 Spectral methods

The most accurate method for solving linear (and most often nonlinear) differential equations is using Fourier transforms, termed in general as *spectral methods*. Apart from solving, a useful application of Fourier transforms is in studying the spectral decomposition, or power spectrum, i.e, distribution of energy in different possible modes. Consider the diffusion equation

$$\frac{\partial y}{\partial t} = D\frac{\partial^2 y}{\partial x^2}. \tag{6.5}$$

The (ODE inspired) solution is given by

$$y(t,x) = e^{Dt\frac{\partial^2}{\partial x^2}} y(0,x). \tag{6.6}$$

Taking cue

$$y(\Delta t,x) = e^{D\Delta t\frac{\partial^2}{\partial x^2}} y(0,x). \tag{6.7}$$

Recall

$$\mathcal{F}_k(\frac{\partial}{\partial x}y(x)) = -iky(k), \tag{6.8}$$

and consequently

$$y(\Delta t,x) = \mathcal{F}_k^{-1}\mathcal{F}_k(e^{D\Delta t\frac{\partial^2}{\partial x^2}} y(0,x)) \tag{6.9}$$

$$= \mathcal{F}_k^{-1}(e^{-Dk^2\Delta t}Y_k). \tag{6.10}$$

Optimal routines for (fast) Fourier transforms are a professional exercise in themselves and better left to professionals. The practice is to use these packages (many available free such as LAPACK, NAG, IMSL,etc.,.), and *call* them as and when required.

Chapter 7

Random systems

Stat. mech. deals with systems of large($\to \infty$) degrees of freedom. Say, a box of gas molecules. This is a *deterministic* system in principle. But practically it is impossible to track the motion of all particles forming the gas, neither theoretically nor experimentally. If we color one of the molecules in the gas, then its motion, due to the frequent collisions with other members, will resemble a random behavior. The same trait can be seen in every system in statistical physics. In order to replicate this system, or to estimate any worthwhile physical quantity of the system, it is essential that we be able to replicate random behavior.

The first tool in studying a statistical system numerically is the

7.1 Random number generator

The computer is a classical machine. Unless told how to do so, it cannot generate a (random) number. However, for our purpose it suits to have a *pseudo*-random number (at least most of the times). We have seen one instance earlier on how a sequence of such numbers can be generated when we discussed forced pendulum with damping (see Sec. 3.2). There we noted that for certain values of forcing amplitude the motion was *chaotic* (see Figure 3.2). Using such a system if one were to start with a certain initial value $\theta_0 = \theta(0)$ (the *seed*), we obtain a random looking sequence $\theta(T),\ \theta(2T), ...$ for some T. This is a *pseudo*-random sequence, for the seed determines the sequence. Repeating the iterations with the same seed one gets the same *random* sequence. Another little issue which is not so transparent, is the distribution of these random numbers. For a fair random sequence, we expect the distribution to be uniform through its entire range for large N, such as saying that a fair coin has the same probability of head or tail. The chaotic system usually chosen for the purpose is a relative of the logistic map, given by

$$x_{n+1} = (ax_n + b)_{mod\ m}, \tag{7.1}$$

for values of a, b and $m(= 16\ or 32)$ chosen apriori. The value of x_0 acts as the seed. The sequence thus generated is known to have a uniform distribution in the range $0 \leq x_n < m$.

7.2 A different choice of distribution

Often it is required to a have a distribution function other than the uniform distribution we discussed in section 7.1. Starting with a uniform random sequence obtained above, we can modify, or chip the distribution to a desired one in two ways:

Method 1. Transformation method: Let $\{x_0, x_1...\}$ be a random sequence with distribution $P_x(x)$. Let $y = y(x)$ lead to a sequence $\{y_0, y_1, ...\}$ with the desired distribution function $P_y(y)$. Then,

$$P_x(x)dx = P_y(y)dy, \tag{7.2}$$

by sheer number conservation. Thus, if $[x_i]$ were a sequence with uniform distribution ($P_x(x) = 1/(x_{max} - x_{min})$), then

$$P_y(y) = \frac{1}{x_{max} - x_{min}}(\frac{dy}{dx})^{-1}. \tag{7.3}$$

Exercise 7.1: *Using Eq. (7.3), show that for a random sequence in the range* $(0, 1)$ *with Poisson distribution* ($P_y = e^{-y}$), $y = -ln(x)$.

Method 2. Rejection method: Method 1 works only when the P_y is a simple function that can be integrated out. A rejection method works even in the case of an arbitrary P_y such as the one in Figure 7.1. Say, the range is divided into small bins containing the random numbers in that range. Elimination method effectively removes a certain number of "numbers" from each bin depending on the probability P_y corresponding to each bin. Let $[x_i]$ be a random sequence with uniform distribution. The rejection method proceeds thus:

$$\begin{aligned}
&find \;\; P_{y,max} \\
&(P_{y,max} = maximum \;\; value \;\; of \;\; P_y(y_i)) \\
&generate \;\; uniform \;\; rnd \;\; sequence \;\; [p_i], 0 \leq p_i \leq P_{y,max} \\
&for \;\; i = 0....(N-1) \\
&find \;\; P_y(y_i) \\
&if \;\; P_y(y_i) < p_i \;\; reject \;\; y_i \\
&do \;\; for \;\; all \;\; i
\end{aligned}$$

Exercise 7.2: *Use the rejection method to obtain a random sequence with a Gaussian distribution* $P_y = B\exp[(y - y_c)^2/\sigma^2]$, *centered at* y_c, *of width* σ, *and* B *is a suitable normalization factor.*

7.3 Monte Carlo integration

A uniformly distributed random sequence can be used to perform integration by a Monte Carlo method. The idea: Consider a closed region enclosed in, say, a square. If we choose a (uniformly distributed) random sequence of points in the square, then the area of the closed region of interest is proportional to the total number of points in the region. Evidently the accuracy of the method

increases with the total number of points N. The accuracy in this method goes as $\sim N^{-1/2}$. Interestingly it is independent of the dimension. On the other hand the Simpson's rule has the accuracy going as $\sim N^{-2/d}$. Consequently, the Monte Carlo method works better in higher dimensions.

Exercise 7.3: *Estimate the area covered by the function* $-0.5+exp(-x^2)$ *over the x-axis, using random number generator.*

7.4 The Random walk problem

As stated in the introduction, if we were to color one specific particle in a volume of gas, and observe its motion, it will essentially look Brownian. The kicks and jolts from its neighboring brethren will lead our colored particle to a *random walk* miming a *drunkard*. For a start we consider a random walk in 1-D.

Let the drunkard start at the origin, and be allowed randomly to take a step either right or left. To simulate the drunkard we use a random number generator (with uniform distribution) in the range $[0, 1)$. For each such random number we move left or right if the number is < 0.5, or ≥ 0.5 respectively.

$$\begin{aligned} for \quad & k = 0, 1, 2, ...n \\ & i = 0; \\ rnd(p) \quad & //p \in [0, 1) \\ if(p < 0.5) \quad & i++ \\ if(0.5 \leq p < 1) \quad & i-- \\ repeat \quad & for \quad k \end{aligned}$$

The final position of the walker is i. A quantity of interest is the distance x the drunkard would have moved from the center. On an average, over large number of such walks, the distance moved would be '0'

$$< x_n >= 0, \tag{7.4}$$

since he is equally likely to have moved either way. Alternately, the mean square displacement is linear in time

$$< x_n^2 >= Dt. \tag{7.5}$$

7.5 Self avoiding walk(SAW)

In several examples however, it is necessary to incorporate the condition of *self avoiding walk*, i.e., two successive steps cannot be in the same direction. Evidently this makes the problem trivial in 1-D. However, there is some head room in 2-D. Examples include drug design, polymer formation, etc., where a *step* is an addition of a molecular bond. An extra condition is that a site once visited (a site where a molecule exists already) cannot be visited again.

Similar to the random walk problem Sec. 7.4, we repeat the same process:

$$\begin{aligned} for \;\; k &= 0, 1, 2, ...n \\ i &= 0; \;\; j = 0 \\ rnd(p) \;\; &//p \in [0, 1) \\ if(p < 0.25) \;\; &i++ \\ if(0.25 \leq p < 0.5) \;\; &i-- \\ if(0.5 \leq p < 0.75) \;\; &j++ \\ if(0.75 \leq p < 1) \;\; &j-- \\ repeat \;\; for \;\; &k \end{aligned}$$

The final position of the walker is (i, j). Here again, evidently, the average distance over large number of walks is $'0'$

$$< x_n >= 0. \tag{7.6}$$

On the other hand

$$< x_n^2 >= D_2 t^{\alpha}, \tag{7.7}$$

where $\alpha = 1.4$. A peculiar situation in 2-D is getting *cornered* or *locked* with nowhere to go, in spite of unoccupied sites (As in Figure 7.5). A situation that happens less frequently in 3-D (and much

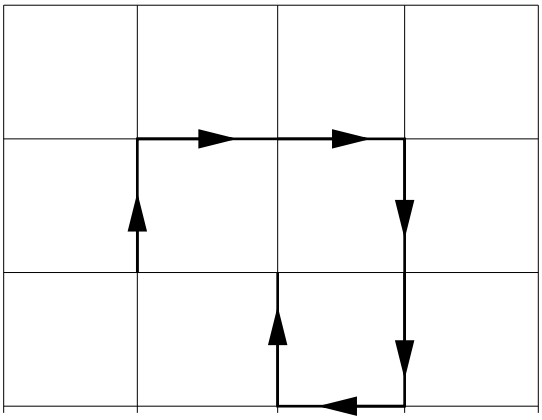

Figure 7.1: A case of a *locked* SAW. The walkers path in the 2-D grid is shown by the arrows. It is easy to imagine similar situations in 3-D, and higher dimensions, but more rarely.

more rarely in 4-D). Consequently, repeating the same SAW in higher dimensions we get smaller values of α, tending to 1 as the dimensionality increases.

Exercise 7.1: *Repeat SAW in 3-D and 4-D, and show that* $\alpha \sim 1.24$ *and* 1.15 *respectively.*

7.6 Random walk and diffusion

The result in Eq. (7.5) has a uncanny resemblance to a certain result in the diffusion problem, given by Fick's (second) law:

$$\frac{\partial \rho}{\partial t} = D\frac{\partial^2 \rho}{\partial x^2}. \tag{7.8}$$

The equation describes, say, the density variation of a drop of ink in a long column of liquid (assumed to be 1-D). If the initial density distbn. is assumed to be in the form of a peaked Gaussian (a delta function), then the solution to the problem is given by

$$\rho(x,0) = \frac{1}{\sigma}\exp(-\frac{x^2}{2\sigma^2}) \tag{7.9}$$

where $\sigma = \sqrt{2Dt}$, implying that the ink diffuses in the liquid in the same way a random walker strolls from the center, *on an average*.

Exercise 7.2: *As an exercise you might try Eq. (7.8) by the methods described in the previous chapters, to see how the density varies in time. Take initial density to be* $1/\sqrt{2D}exp(-x^2/4D)$*, and* $D = 0.5$*.*

7.7 Random walk in 2-D and Entropy

Simulation of a random walk in 2-D is very much along the same lines as that of 1-D. In fact even the results are the same, *vis-a-vis*

$$< x_n^2 >= Dt. \tag{7.10}$$

As a little variation, we start with a total M number of particles at the center, each of which takes a random walk independent of the other. We also let more than one particle occupy a site at a given time. Having realized the connection with diffusion problem, this random walk is effectively a diffusion problem in 2-D. However, we shall be fixated with another quantity, the entropy. Entropy, born out of the ergodic hypothesis, measures disorderliness, and also sets the direction of time. A system, *in its natural course*, moves in the direction of more disorder, i.e., from a ordered state to a more disordered state, and also thus indicating the direction of time. For the problem under consideration, a *microcanonical ensemble*, the entropy of the system of particles after N random steps is given by

$$S(N) = -\sum P_i(N)\ln P_i(N), \tag{7.11}$$

where $P_i(N)$ is the probability of finding the system in microstate i after N steps. If we divide the square grid where the particles take a random walk into boxes labeled $i = 1, 2, 3, ..$ then $P_i(N)$ is simply the number of particles m_i in the ith box divided by M. A plot of S versus time t (or N) shows that the entropy increases till it plateaus out, i.e., it moves to equilibrium where it is extremum. You may notice that this in accordance with the ergodic hypothesis.

7.8 Cluster growth models

A interesting process that is closely related to random walk is the formation of clusters, such as snowflakes, cancer cells or soot particles.

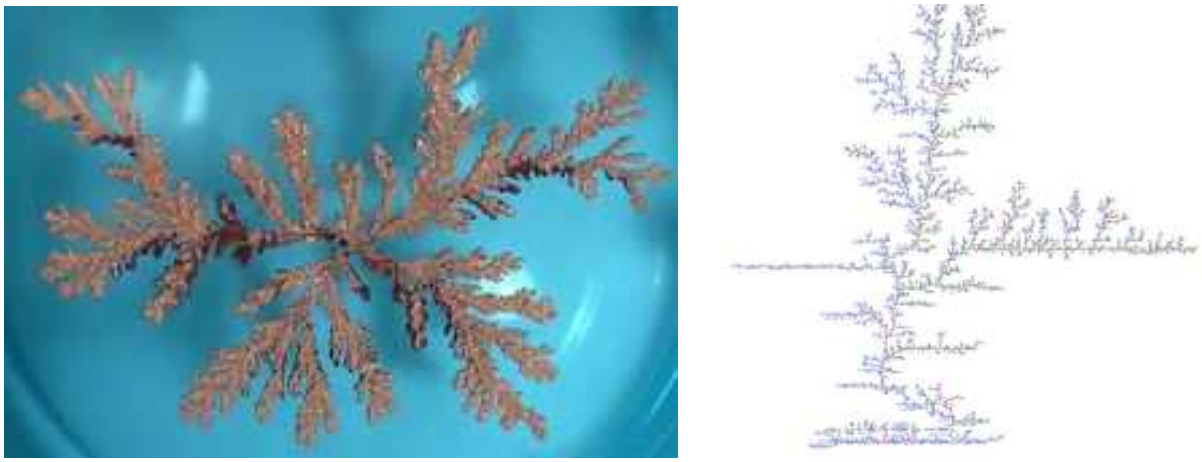

Figure 7.2: A real cluster grown from copper sulphate solutions (left) and a simulated DLA tree (right). (Picture taken from Wikipedia)

Eden model - The rules of formation of a eden cluster is as follows:
1. Consider a 2-D lattice of points (i, j).
2. Start by placing a seed particle at the origin $(0, 0)$. This is the initial cluster. Its nearest neighbors form the perimeter of the seed cluster.
3. The cluster grows by adding particles to the perimeter sites. Pick one of the perimeter sites at random and place a particle at that site. The cluster now consists of two particles and a larger perimeter.
4. Step 3 is now repeated.

Since each of the perimeter sites are treated at par, each site is likely to be filled up sooner or later. The cluster roughly grows as a circle around the seed. The cluster grows from within, expanding its borders and often referred to as the cancer model.

Diffusion Limited Aggregation (DLA) model - Not all clusters grow from within. Snow flakes, soot deposits or smaller particles building up to form a larger particle in a solution are some alternate examples. Formation of these clusters are better explained by the DLA model.
1. As earlier we start with a 2-D lattice and a seed particle at the origin
2. A particle is dropped at a site (i, j) chosen at random. This particle is then allowed to perform a random walk till it attaches to the seed particle.
3. Step 2 is repeated for many particles till a large cluster is formed.

As we have already seen, a random walk is equivalent to a diffusion. A particle at any point on the grid diffuses till it attaches itself to another particle to form a cluster. A important feature of the structure obtained through DLA is that it has a fractal nature. A fractal carries the property

Figure 7.3: A electric discharge in a dielectric forming a fractal structure. (Picture taken from Wikipedia).

of self similarity. I.e., the structure preserves its properties, statistically, at every scale. We shall discuss this in a little more detail, and how to calculate the fractal dimension of a structure, next.

7.9 Fractals and Fractal dimensionality of curves

Recall the way entropy was calculated in Section 7.7. Imagine doing the same calculation on a picture of cloud. I.e., divide the given picture into grids. Adapt a suitable scale to arrive at the cloud occupancy in each grid, and use the expression Eq. (7.11) to calculate the entropy. Now magnify a smaller region in the picture, and repeat the same exercise. Further down, take a small square region in this magnified picture and repeat the entropy calculation for this smaller region. It turns out that entropy calculated is more or less the same. This scale invariance appears to be a chosen feature of several natural structures: coast lines, river maps, etc.,.

A important quantity that characterizes the fractal nature is the fractal dimension of the structure. To calculate the dimension of a fractal structure, we use the following idea: Consider a 3-D structure, such as a sphere. The mass m of the structure goes with the radius as r^3. Similarly, for a circular disk it is r^2, and a linear structure it is r. The dimension of the structure appears as the exponent of the scale. The calculation of the fractal dimension will be along these lines. In the simulated DLA structure in Figure 7.2, we choose small circular discs of different radii at various points on the occupied sites. If we associate a constant mass with each of the occupied location, then the mass of each disc m_i depends on the radius as r^{d_f}, where d_f is the fractal dimension of the structure. A log-log plot of mass vs radius then gives a rough straight line, whose slope then is d_f.

For a structure such as the Koch curve(s), fractal dimension can be calculated analytically. Let us imagine walking along these curves with step lengths L_s, and let L_{eff} be the effective distance we travel in N_s steps. I.e., $L_{eff} = N_s L_s$. For an ordinary curve the length of the cure L_{eff} does not depend on the step size L_s. Or, $N_s \propto L_S^1$. However, for a Koch curve (or any fractal) this is

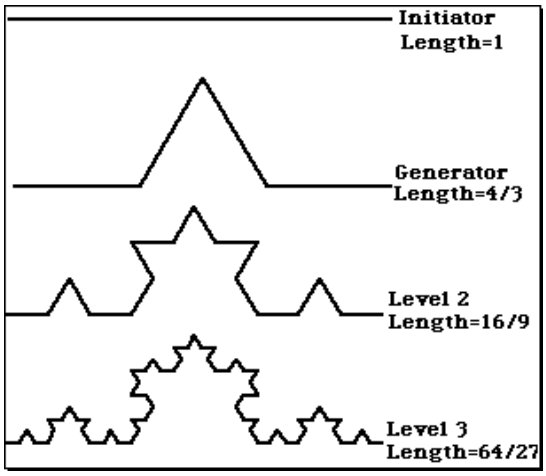

Figure 7.4: A family of Koch curves generated through recursion. The curves are, by construction, scale invariant, or self similar. (Picture taken from Wikipedia).

not true. For a given L_s, we ignore the finer details of the underlying step. Taking smaller steps we walk longer due to the extra visible structure of the fractal. Or, for a fractal $N_s \propto L_s^{-d_f}$. I.e., $L_{eff} = L_s^{1-d_f}$. For the Koch curve in Figure 7.4, d_f can be calculated analytically. For $L_s = 1$, we notice $N_s = 1$. For $L_s = 1/3$, $N_s = 4$. Similarly for $L_s = 1/9$, $N_s = 27$. Consequently, $d_f = \ln 4/\ln 3 \sim 1.262$.

7.10 Percolation

Percolation refers to the filtering or seeping of fluid through a porous medium - water through soil, oil through rock, etc.,. It also forms a good starting model for several other phenomena, such as disease spreading or forest fires. We shall present the problem thus. Consider a forest of trees distributed randomly with density $\rho(0 < \rho < 1)$. Assume we set fire to one of trees at one end, and let T be the time taken for the fire to die out. In a thin forest the fire dies down fast burning down a few trees, whereas for large ρ it can possibly burn down the whole forest. A rough plot $T\ vs\ \rho$ is shown in Figure 7.5. While the behavior is comprehensible for small and large values of ρ, the curious aspect is the singular behavior at a certain value of ρ close to 0.6. Indeed the figure hints a phase transition.

We simulate the forest of density ρ as follows: Construct of square grid of size $N \times N$. We generate a random sequence with uniform distribution $0 \leq x < 1$. At each site (i, j) we place a tree if the random number we pick from the sequence is less than ρ.

$$\begin{aligned} for\ \ i, j = 0, 1, ...N \\ pick\ \ random\ \ number\ \ x,\ 0 \leq x < 1 \\ y(i, j) = 1\ \ if\ \ x < \rho,\ \ else\ \ y(i, j) = 0. \end{aligned}$$

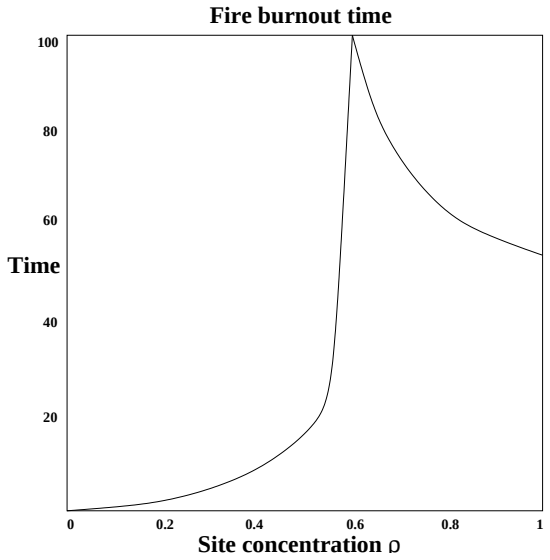

Figure 7.5: A rough sketch of the burnout time *vs* site concentration in a forest. The burnout time shows a phase transition at 0.593.

$y(i,j) = 1$ represents a location in the forest occupied by a tree. We define a cluster as a string of trees connected through nearest neighbors. Thus, a tree with no nearest neighbors is a 1-cluster. Two trees that are nearest neighbors, but with no other nearest neighbors forms a 2-cluster. A n-cluster is a cluster of n trees connected through nearest neighbors. A 'spanning-cluster' is one whose limbs touch all four sides of the forest. The singularity in Figure 7.5 is noticed at around $\rho = 0.593$ when spanning clusters start to appear. The reason for the singularity lies in the fact that a spanning cluster at the critical region has a fractal nature. To keep track of the size of the cluster forms the most nontrivial part of the simulation. As we move along the lattice site, we give a new label to a tree when we place one. If the tree has a nearest neighbor then the label must be the same as the earlier one. Thus each cluster has a separate label. If a newly placed tree happens to connect two different clusters, say integers a and b, then this reduces them to single cluster. The entire cluster must be labeled as the lowest of a and b. At the end of the simulation it must be checked if any of the clusters has ends at all four sides of the lattice.

To see the fractal nature of the spanning cluster, one such cluster can be directly generated. We start by placing a seed at the origin. For the spanning cluster to form the points adjacent to this seed will be occupied with probability ρ. We make a list of nearest neighbor sites and move to each of the nearest sites and populate them with probability ρ. A site that is not chosen for occupancy is eliminated from the list, while a newly occupied site brings in additional sites to the list. It is noted that for $\rho < \rho_c (= 0.593)$ no spanning clusters are formed. For large values of ρ every occupied site is very likely to be part of one large cluster. For $\rho \sim \rho_c$, spanning clusters resembling DLA clusters form. However, the have a different fractal dimension (~ 1.9).

The behavior of the burnout time in Figure 7.5 can now be explained (It must be remembered that the burnout time must be understood in an average sense). For small values of concentration the clusters are mostly small in size, and consequently the burnout time is small. At the critical

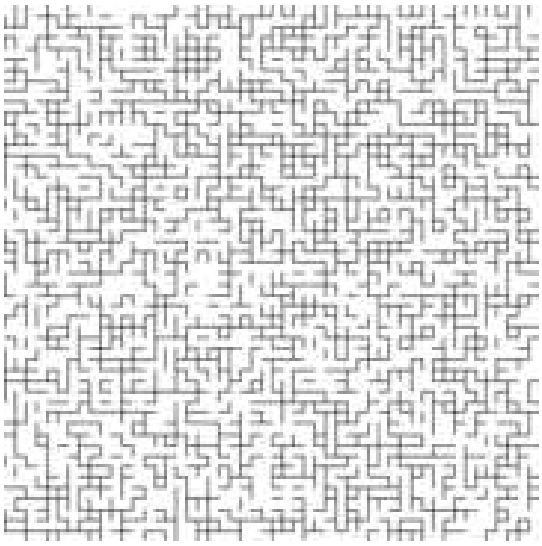

Figure 7.6: A family of Koch curves generated through recursion. The curves are, by construction, scale invariant, or self similar. (Picture taken from Wikipedia).

value of concentration, the cluster has a fractal structure. Consequently, the fire takes a lengthy and tedious path within the grid, and hence a long time. For large values of concentration each tree has almost all neighboring sites populated. This results in the fire spreading fast in all directions, burning down the forest faster than at criticality.

Chapter 8

Statistical Mechanics

Contemporary statistical mechanics concerns largely with the phases of matter. The questions centered around how a measured property of a system be related to a gross property of a large number of subsystems. However, over the last few decades the agenda has widened to include several branches where the statistical methods are directly applicable. Some examples are evolutionary biology, financial markets, game theory, neural networks and problems in biology such as protein folding and DNA denaturation. Simulations form the primary back bone in understanding these problems. In this chapter we discuss the primary method of Monte Carlo simulation as applied in studying phase transition in the Ising model - a simplified version of a ferro(anti-ferro) magnet.

8.1 The Ising Model

The model assumes the magnet to be a lattice of spins that interact only with their nearest neighbors. Further the spins can take only either of the two values ± 1. The hamiltonian of the system is given by

$$H = -J \sum_{<i,j>} \mathbf{S}_i \mathbf{S}_j, \quad \mathbf{S}_{i,j} = \pm i. \tag{8.1}$$

$J > 0 (J < 0)$ for ferro(anti-ferro) magnets. The notation $< i, j$ indicates that the sum is over nearest neighbors. The model is a simplified version of the Heisenberg model for a lattice of spin *vectors* given by

$$H = -\frac{1}{2} \sum_{i,j} (J_1 S_{xi} S_{xj} + J_2 S_{yi} S_{yj} + J_3 S_{zi} S_{zj}). \tag{8.2}$$

When $J_3 >> J_2, J_1$, the model approximates to the Ising model.

8.2 Mean field theory

A sketch of a lattice of spins in a square lattice in 2-D is shown in Figure 8.1. A specific configuration of the spins, such as the one in Figure 8.1 will be referred to as a *microstate*. The preference of the system is for all the spins to be parallely aligned, as this is energetically favored. However,

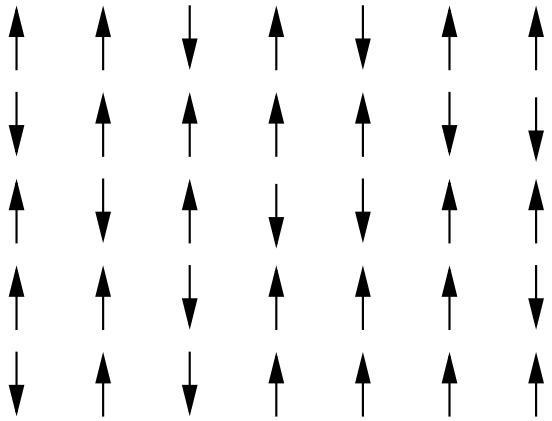

Figure 8.1: The Ising model consists of 'up' or 'down' spins at each lattice site. The figure shows one possible microstate of the system. At thermal equilibrium with temperature T, the system flip-flops through several microstates, with probability P_i proportionate to the Boltzmann factor $exp(-E_i/kT)$, where E_i is the energy of the microstate.

as the temperature of the system is increased the scenario changes. If the system is at thermal equilibrium at temperature T, i.e., it is in contact with a heat bath at T, the state of the system goes through several microstates as time progresses. The probability of the system being in a particular microstate i of energy E_i is given by the Boltzmann factor

$$P_i \propto e^{-E_i/kT}. \tag{8.3}$$

Over a time period the system at temperature T goes through several microstates. The measured value of a physical quantity, say magnetization M is then the time average over these microstates. Since the ergodic hypothesis guarantees the equivalence of *ensemble average* and *time average*, we have

$$M = \sum_i P_i M_i, \tag{8.4}$$

where M_i is the value of magnetization in the microstate i.

To see how magnetization changes as a function of temperature we shall first consider a paramagnet in the presence of a magnetic field B, whose hamiltonian is given by

$$H = -\mu \sum_i B S_i. \tag{8.5}$$

The probability of each spin being aligned along (or opposite to) B is

$$P_{+(-)} = \frac{e^{+(-)\mu B/kT}}{e^{\mu B/kT} + e^{-\mu B/kT}}. \tag{8.6}$$

Thus average magnetization of the i'th spin is given by

$$\begin{aligned} < S_i > &= P_+ - P_- \\ &= tanh(\mu B/kT). \end{aligned} \tag{8.7}$$

We rewrite the Ising hamiltonian Eq. (8.1) as

$$H = -(J \sum_{<i,j>} S_j)S_i = -\sum_i B_{eff} S_i, \tag{8.8}$$

i.e., we assume the ith spin to be acted upon by the mean field due to its neighboring spins. Now we make the (mean field) approximation that for a large system the average behavior of ith spin is as good as any other. I.e.,

$$< S_i >=< S_j >=< S > . \tag{8.9}$$

Substituting these results in that of the paramagnet we have

$$< S >= tanh(Jz < S > /kT), \tag{8.10}$$

where z is the number of nearest neighbors. In a n-D square lattice $z = 2n$. Approximating $tanh(x) = x - x^3/3$ we get

$$< S >= \frac{zJ < S >}{kT} - \frac{1}{3}(\frac{zJ < S >}{kT})^3 \tag{8.11}$$

with solutions $< S >= 0$ and

$$< S >= \sqrt{\frac{3}{T}(\frac{kT}{zJ})^3}(\frac{zJ}{k} - T)^{1/2} \sim (T_c - T)^{\beta} \tag{8.12}$$

where $\beta = 1/2$ is a critical coefficient. The second solution implies that a $T < T_c$ the magnetization $< S >$ has a nonzero value, thus showing a phase transition.

8.3 Newton's method

Equation (8.10) is a transcendental equation. If we define

$$f(x) = x - tanh(ax), \tag{8.13}$$

solving Eq. (8.10) is equivalent to finding x_0 such that $f(x_0) = 0$. To do this (or solve any algebraic equation) we employ the Newton's method. Let x_0 be solution we seek. We start with a seed solution x_1. If $x_0 = x_1 + \Delta x_1$ then,

$$f(x_0) = f(x_1 + \Delta x_1) = f(x_1) + f_x(x_1)\Delta x_1 \tag{8.14}$$

Since $f(x_0) = 0$, this implies

$$\Delta x_1 = -\frac{f(x_1)}{f_x(x_1)}. \tag{8.15}$$

Using Δx_1 we find a new value for the seed, $x_2 = x_1 + \Delta x_1$. The solution is obtained by repeating this iteration till a tolerance level is reached.

8.4 The Monte Carlo Method

At equilibrium the Ising system goes through a series of microstates in time. In order to compute the measured value of a physical quantity, we need to simulate these microstates. An average over these microstates of the physical quantity in question then gives its measured value. The probability of occurrence of a particular microstate i with energy E_i is given by the Boltzmann factor.

The simulation of these microstates in a grid of size $N \times N$ goes along the following algorithm. Initially we choose a microstate, say, with all spins up. We take $\Delta E_{i,j}$ to be the energy associated with the flipping of the Ising spin $S_{i,j}$ at site (i, j). Then, if $\Delta E_{i,j} < 0$, the spin $S_{i,j}$ is flipped, as this is a energetically favored transition. Otherwise, the flip occurs with a probability $P_\alpha \propto exp(-\Delta E_{i,j}/kT)$. To do this we generate a (uniformly distributed) random number $0 \leq x < 1$. The spin is flipped if $x < exp(-\Delta E_{i,j}/KT)$. The algorithm is outlined below:

$$
\begin{aligned}
&chose\ \ any\ initial\ \ microstate\ S_{i,j}\ \ in\ \ sites(i,j)\\
&\qquad\qquad for\ i,j = 0....N\\
&\qquad\qquad if\ \Delta E_{i,j} < 0\ then\ S_{i,j} = -S_{i,j}\\
&\qquad\qquad if\ \Delta E_{i,j} >= 0\ then\\
&\qquad\qquad\qquad \{\\
&\qquad\qquad\qquad pick\ random\#x\\
&if\ x < exp(-\Delta E_{i,j}/kT)\ then\ S_{i,j} = -S_{i,j}\\
&\qquad\qquad\qquad \}
\end{aligned}
$$

Simulation methods that involve decision making based on a dice throw, or a random number, is generally referred to as Monte Carlo methods. The flipping (or not) of a single spin is referred to as a single *Monte Carlo time step*. The simulation repeated over several time steps till all spins in the grid are given a chance to flip. This gives a single microstate. This is repeated to generate several microstates before the sought averages over microstates are taken. The magnetization $< M >$ obtained using these simulations show a clear non-zero value for temperatures below a certain temperature T_C. Above T_C the average goes to zero. At values close to T_C, the average shows strong volatility, signifying a phase transition.